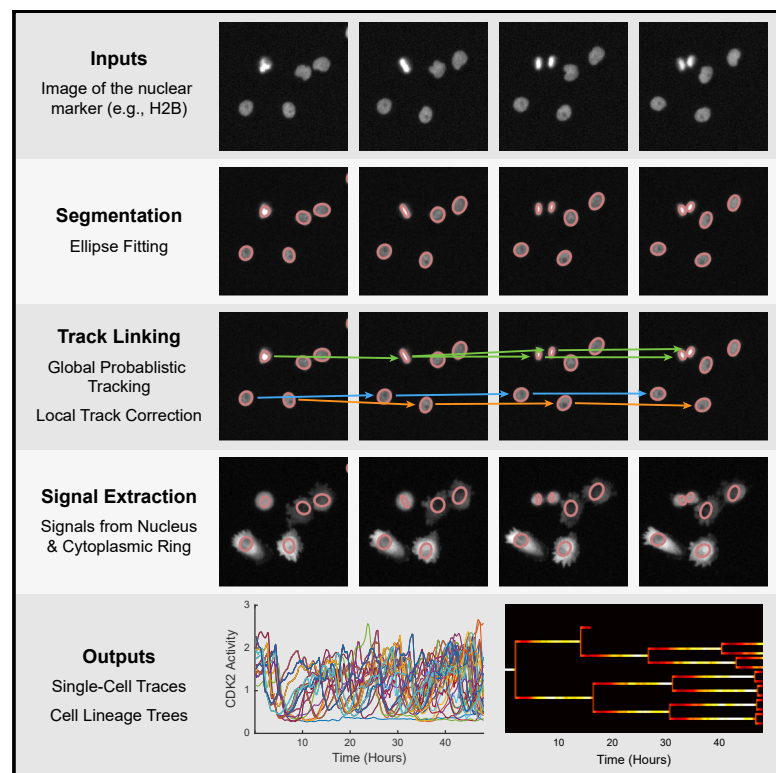


# EllipTrack: A Global-Local Cell-Tracking Pipeline for 2D Fluorescence Time-Lapse Microscopy

## Graphical Abstract



## Authors

Chengzhe Tian, Chen Yang,  
Sabrina L. Spencer

## Correspondence

chengzhe.tian@colorado.edu (C.T.),  
sabrina.spencer@colorado.edu (S.L.S.)

## In Brief

Tian et al. present a cell-tracking pipeline called EllipTrack that is optimized for modern, multi-day, high-throughput 2D fluorescent time-lapse movies. EllipTrack produces nearly error-free cell lineages for the cell lines tested and represents an improvement over existing tools for hard-to-track cells such as cancer cells.

## Highlights

- EllipTrack applies ellipse fitting to separate partially overlapped cells
- EllipTrack utilizes a global-local hybrid algorithm to map cells between frames
- EllipTrack can track cell lineages in long-term movies with minimal errors
- EllipTrack accelerates discovery in cell biological and pharmacological research



## Report

# EllipTrack: A Global-Local Cell-Tracking Pipeline for 2D Fluorescence Time-Lapse Microscopy

Chengzhe Tian,<sup>1,3,4,\*</sup> Chen Yang,<sup>2,3,4</sup> and Sabrina L. Spencer<sup>1,3,5,\*</sup><sup>1</sup>Department of Biochemistry, University of Colorado Boulder, Boulder, CO 80303, USA<sup>2</sup>Department of Molecular, Cellular, and Developmental Biology, University of Colorado Boulder, Boulder, CO 80303, USA<sup>3</sup>BioFrontiers Institute, University of Colorado Boulder, Boulder, CO 80303, USA<sup>4</sup>These authors contributed equally<sup>5</sup>Lead Contact\*Correspondence: [chengzhe.tian@colorado.edu](mailto:chengzhe.tian@colorado.edu) (C.T.), [sabrina.spencer@colorado.edu](mailto:sabrina.spencer@colorado.edu) (S.L.S.)<https://doi.org/10.1016/j.celrep.2020.107984>

## SUMMARY

Time-lapse microscopy provides an unprecedented opportunity to monitor single-cell dynamics. However, tracking cells for long periods remains a technical challenge, especially for multi-day, large-scale movies with rapid cell migration, high cell density, and drug treatments that alter cell morphology/behavior. Here, we present EllipTrack, a global-local cell-tracking pipeline optimized for tracking such movies. EllipTrack first implements a global track-linking algorithm to construct tracks that maximize the probability of cell lineages. Tracking mistakes are then corrected with a local track-correction module in which tracks generated by the global algorithm are systematically examined and amended if a more probable alternative can be found. Through benchmarking, we show that EllipTrack outperforms state-of-the-art cell trackers and generates nearly error-free cell lineages for multiple large-scale movies. In addition, EllipTrack can adapt to time- and cell-density-dependent changes in cell migration speeds and requires minimal training datasets. EllipTrack is available at <https://github.com/tianchengzhe/EllipTrack>.

## INTRODUCTION

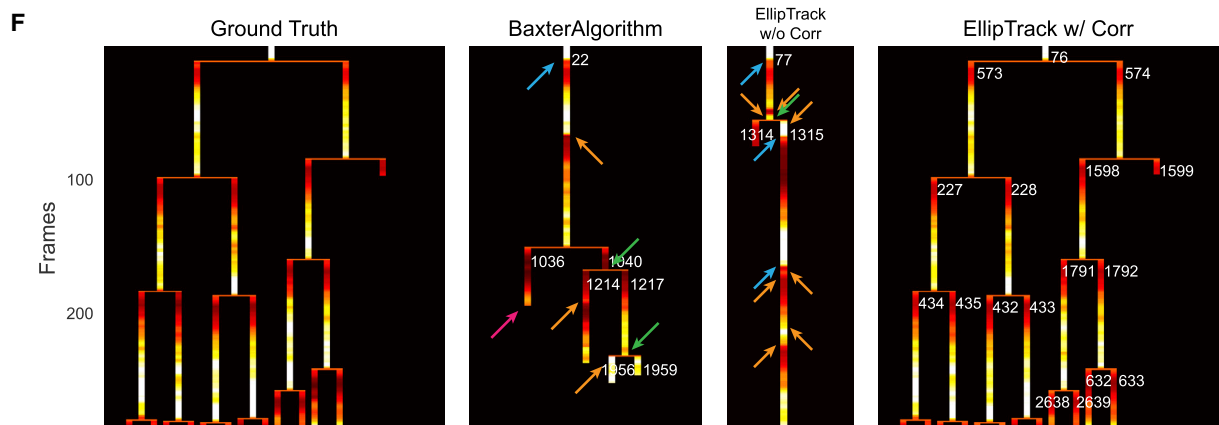
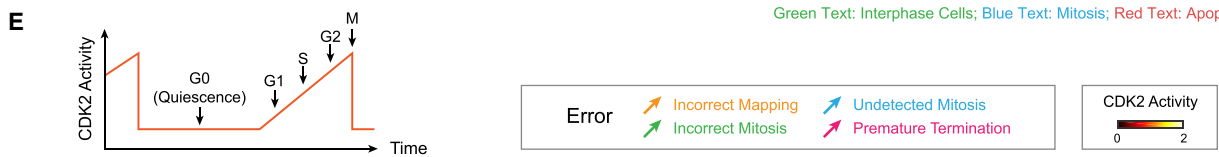
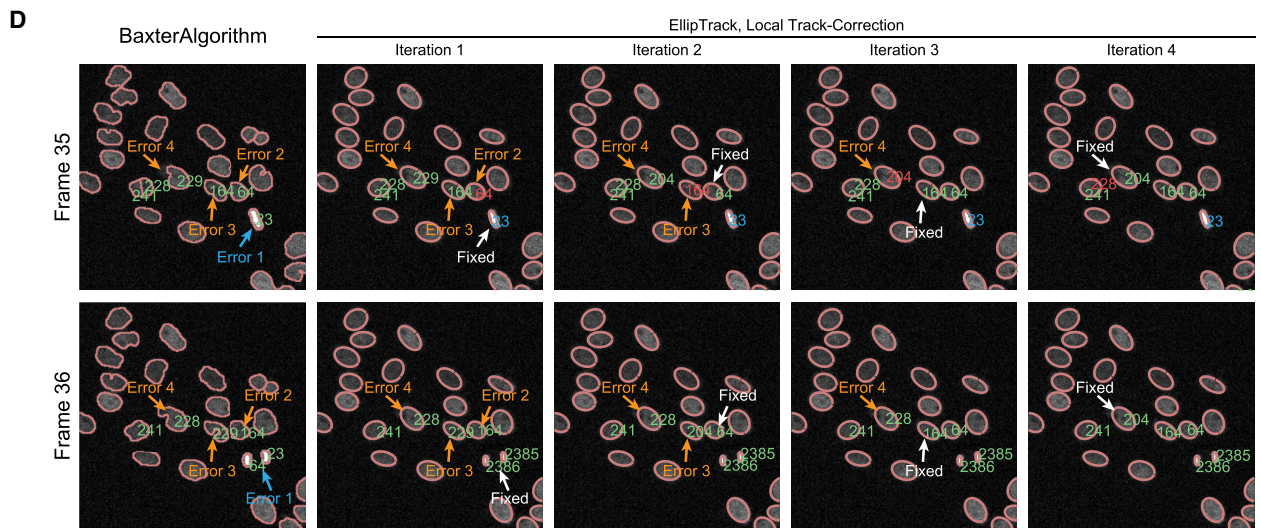
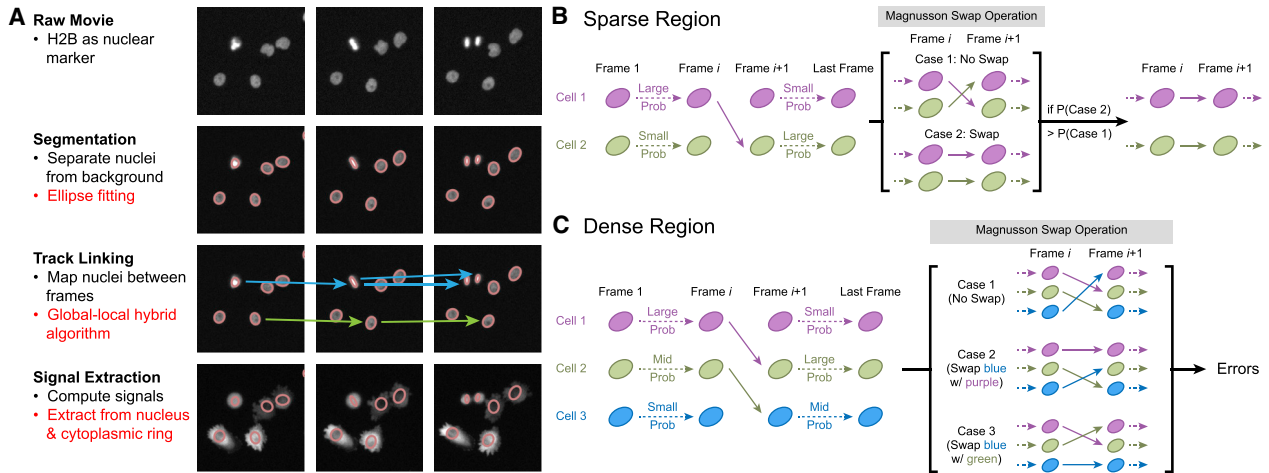
Biological processes are highly dynamic and display varying degrees of cell-to-cell heterogeneity. Time-lapse imaging enables analysis of single-cell dynamics, providing longitudinal information that is not readily accessible by other single-cell methods. In a typical 2D fluorescence time-lapse microscopy experiment, cells are labeled with fluorescent markers for the signals of interest and imaged periodically under a microscope to generate a movie. A computational tool (hereafter referred to as a “cell tracker”) is then applied to the movie to track cells over time and extract signals from each cell (Kudo et al., 2018). Because of its ability to visualize molecular activities in living cells in real time, time-lapse microscopy has been used to study a wide range of biological questions.

A classical cell tracker typically consists of three steps (Figure 1A). First, in segmentation, cell nuclei are identified from the images with a fluorescent nuclear marker, such as histone 2B (H2B). Then, in track linking, nuclei are mapped between neighboring frames and biological events, such as mitosis and apoptosis, are identified. Finally, in signal extraction, signals are extracted from the regions of interest in each cell to gain biological insights. During the past decade, enormous effort has been made to improve the accuracy of each step (He et al., 2017; Hernandez et al., 2018; Maška et al., 2014; Moen et al., 2019; Ulman et al., 2017). Some cell trackers also attempt to perform segmentation and track linking jointly, such that the properties of cell tracks

from previous frames can be used as prior information to track later frames (Amat et al., 2014; Arbelle et al., 2018; Cappell et al., 2016). Despite these efforts, cell tracking remains a bottleneck in the field of time-lapse microscopy because of the necessity of achieving extremely high accuracy at each frame (Skylaki et al., 2016). Consequently, manual verification and correction is often required (Han et al., 2019; Hilsenbeck et al., 2016), which limits the scale of experiments and results in large amounts of data remaining unextracted and unquantified.

A major breakthrough in cell tracking was the creation of the global track-linking algorithm by Magnusson et al. (2015), which aims to construct cell tracks by maximizing the overall probability of cell lineages. Here, a cell track maps a cell in every movie frame from its appearance to its disappearance, and a cell lineage is a tree of cell tracks representing mother/daughter relationships. To do so, this algorithm first uses machine learning tools to infer the probability of cell overlapping, cell migration, and other biological events (mitosis, apoptosis, etc.). It then uses the Viterbi algorithm to iteratively search for and assemble the cell track that results in the greatest increase in the probability of existing cell lineages, until this probability can no longer be improved. Because of its consideration of the entire movie, rather than only two neighboring frames, this algorithm has been consistently rated as a top performer in the Cell Tracking Challenge (Maška et al., 2014; Ulman et al., 2017) and has been implemented in several cell trackers (Cooper et al., 2017; Hernandez et al., 2018; Magnusson et al., 2015).





(legend on next page)

However, the use of the Viterbi algorithm is also a major source of tracking mistakes. Consider two neighboring cells between two neighboring frames (frame  $i$  and  $i + 1$ ) in which the first cell's track before frame  $i$  contributes a much greater increase to the overall probability of cell lineages than the second cell's track, but its track after frame  $i + 1$  contributes less (Figure 1B). Because the aim is to find the cell track leading to the greatest increase in the overall probability, this algorithm will map the first cell in frame  $i$  to the second cell in frame  $i + 1$ , despite the sub-optimal probability between these two frames. Subsequently, the second cell in frame  $i$  will be forced to map to the first cell in frame  $i + 1$ . To fix that mistake, Magnusson et al. (2015) introduces a swap operation: when constructing a new cell track for cell 2, the algorithm will swap this cell track with an existing one (cell 1) if it leads to an increase in the overall probability of cell lineages (Figure 1B). Although this operation works well for small-scale movies, such as those in the Cell Tracking Challenge in which cells are sparsely populated (or more precisely, in which cells migrate significantly slower than the average distance between cells), it is ineffective for modern terabyte-scale movies at the forefront of the time-lapse microscopy field in which cells are continuously imaged on a multi-well plate for many days. In these movies, cells undergo multiple rounds of mitoses, such that the last frame contains up to thousands of cells, and that high cell density often results in multiple neighboring cells being mis-tracked by the Viterbi algorithm at the same frame. Because the swap operation only allows the newly constructed cell track to be swapped with one existing track, it can only correct a fraction of the mistakes. For example, consider the scenario with three neighboring cells in which the first cell in frame  $i$  is mapped to the second cell in frame  $i + 1$ , and the second cell is mapped to the third cell (Figure 1C). When tracking the third cell, no matter which existing track it swaps with, the algorithm will only be able to fix at most one mistake, and the resulting cell lineages are still erroneous (Figure 1C). Therefore, developing an optimized swap operation that corrects mistakes in the densely populated regions is necessary.

Here, we present EllipTrack, a global-local hybrid cell-tracking pipeline. The key innovation of EllipTrack is the user-friendly packaging of the best existing algorithms combined with new local track-swapping algorithms that are executed after the Magnusson et al. (2015) global track-linking algorithm. Our local track-correction algorithms (hereafter called the "local track-correction module") optimize the Magnusson et al. (2015) swap operation and offer a significantly higher capacity to correct tracking mistakes, especially for modern multi-day, large-

scale movies with densely populated cells. Through benchmarking, we show that EllipTrack outperforms current state-of-the-art methods. We also demonstrate the practical aspects of EllipTrack, such as the ability to infer time- or cell-density-dependent migration speeds and the small amount of training data required.

## RESULTS

### The EllipTrack Pipeline

EllipTrack implements the traditional three-step procedure, but introduces multiple advanced features (Figures 1A and S1A). During segmentation, EllipTrack approximates the shapes of cell nuclei as ellipses and segments cells by applying an ellipse-fitting algorithm to the nuclear contours (Zafari et al., 2015). This method shows improved performance in separating overlapping nuclei and has been implemented in other cell trackers (Turetken et al., 2017) (Figure S1B). In track linking, EllipTrack first constructs cell lineages with the Magnusson et al. (2015) global track-linking algorithm and then executes our local track-correction module to correct tracking mistakes (detailed below). Finally, during signal extraction, EllipTrack calculates the signals from the nuclear and cytoplasmic ring regions of each ellipse. Signals are extracted only from the pixels that do not overlap with those of other cells to avoid interference from neighboring cells (Figures S1C and S1D).

The local track-correction module consists of multiple steps, each addressing a different aspect of tracking mistakes. The core step optimizes the Magnusson et al. (2015) swap operation to fix the mistakes in densely populated regions, illustrated in Figure 1C. Because of combinatorial explosion, it is difficult to correct all erroneous cell tracks simultaneously. Instead, we use an iterative strategy in which tracking mistakes are progressively fixed. In each iteration, the core step examines every two cell tracks between every two neighboring frames (i.e., a local algorithm) and determines whether there exists an alternative track configuration that will increase the probability of cell lineages over a pre-defined threshold fold-change (Figure S1E). If so, the alternative with the greatest fold-change will replace the existing configuration. Because the threshold is often much greater than one, the main features of the Magnusson et al. (2015) global track-linking algorithm will be kept and only the significant mistakes will be corrected, thus achieving a balance between the global track-linking algorithm and the local track-correction module (i.e., a global-local algorithm). This process will then repeat until no more changes to the cell lineages can be made.

### Figure 1. The EllipTrack Pipeline

(A) Workflow of cell trackers. Red text indicates the methods implemented in EllipTrack.

(B) Schematic illustration of the Magnusson et al. (2015) swap operation.

(C) Schematic illustration of the limitation of the Magnusson et al. (2015) swap operation for cells in densely populated regions.

(D) Correction of the tracking mistakes of the BaxterAlgorithm by the local track-correction module of EllipTrack. Tracking mistakes are indicated by the orange (incorrect mapping) or blue (undetected mitosis) arrows. Fixed errors are indicated by the white arrows at the iteration in which they are fixed and are removed in later iterations. Track IDs of EllipTrack are adjusted such that unmodified cell tracks always receive the same ID. For EllipTrack, tracks 241 and 228 map to the same ellipse. Dataset: MCF10A-1.

(E) Schematic illustration of classifying cell-cycle phases based on CDK2 activity.

(F) Comparison of identified cell lineages with different cell trackers. Cell lineages are visualized in heatmaps as described previously (Wolff et al., 2018) and colored by CDK2 activity. Track IDs are plotted next to the births of their respective cells, except in the final frames because of space constraints. Arrows indicate tracking mistakes, as explained in the legend. The "density" option was used to infer cell migration speeds over time. Dataset: MCF10A-1.

In addition to the core step, the local track-correction module also fixes tracking mistakes related to under-segmentation, over-segmentation, and undetected mitosis events, as detailed in the [STAR Methods](#).

### EllipTrack Identifies Nearly Error-Free Cell Lineages

To test the power of our local track-correction module, we selected a cell tracker called BaxterAlgorithm as the sample implementation of the [Magnusson et al. \(2015\)](#) global track-linking algorithm and applied it to a 48-hr sample movie of untreated MCF10A mammary epithelial cells expressing a nuclear marker (H2B) and a cell-cycle marker (CDK2 sensor) ([Spencer et al., 2013](#)). We then imported the tracking results to EllipTrack and examined whether our local track-correction module could fix the mistakes made by BaxterAlgorithm. As shown in [Figure 1D](#), we visualized the segmentation outcomes by plotting the contours of identified nuclei on top of the image of the H2B channel. We also displayed the numeric identifiers (IDs) of selected cell tracks next to the nuclei to which they mapped. Track IDs for interphase cells are green, whereas a blue or red track ID indicates that the corresponding cell undergoes mitosis or apoptosis, respectively. As shown in the first column, the BaxterAlgorithm incorrectly tracked multiple neighboring cells, including not detecting the mitosis event of track 23, and mapping tracks 228, 229, 164, and 64 to the incorrect neighboring cells. This is a typical example of tracking mistakes in densely populated regions in which the [Magnusson et al. \(2015\)](#) swap operation is ineffective. In comparison, EllipTrack fixed all those mistakes with its local track-correction module within four iterations ([Figure 1D](#), columns 2–5). In the first iteration, the mitosis event of track 23 was correctly detected, and track 64 was terminated at frame 35. Next, track 164 and 64 were swapped at frame 35 such that track 64 was now correctly tracked and track 164 was terminated. This process was repeated in the last two iterations to fix all mistakes. Thus, our local track-correction module is capable of correcting mistakes that were overlooked by the BaxterAlgorithm.

We next examined the ability of the entire EllipTrack pipeline to identify error-free cell lineages. To that end, we applied EllipTrack (both with and without local track-correction) and the BaxterAlgorithm to the previously mentioned MCF10A movie and visualized the identified cell lineages on signal-based heatmaps. Here, we selected CDK2 activity as the signal of interest with CDK2 activity calculated as the ratio of the cytoplasmic ring signal relative to the nuclear signal of the DNA helicase B (DHB)-based sensor ([Spencer et al., 2013](#)) ([Figure S1F](#)). This sensor is a widely used indicator of cell-cycle progression because CDK2 activity is absent in quiescent (G0) cells and gradually increases throughout G1, S, and G2 phases of the cell cycle. Mitosis can be marked by a rapid drop in CDK2 activity ([Spencer et al., 2013](#)) ([Figure 1E](#)). Therefore, it is possible to evaluate the quality of identified cell lineages by examining whether they match the expected CDK2 activity. As shown in [Figure 1F](#), with tracking results of this lineage visualized in [Video S1](#), both the BaxterAlgorithm and EllipTrack before local track correction made numerous mistakes. For example, both trackers assigned multiple incorrect mitosis events (green arrow), as visualized by a split of cell lineages without the charac-

teristic rise and fall of CDK2 activity. In comparison, the cell lineage identified by EllipTrack after local track correction matched the ground truth established via manual tracking.

Finally, we performed a systematic benchmark of EllipTrack against the BaxterAlgorithm and two other popular cell trackers: iLastik ([Berg et al., 2019](#); [Sommer et al., 2011](#)) and a cell tracker from [Cappell et al. \(2016, 2018\)](#) (also refer to [Chung et al., \(2019\)](#)) ([Table S1](#)). We evaluated their performance on six different movies from multiple sources that well represent current real-world cell-tracking problems, including three movies of cancer cells (HeLa and A375), one movie of cells under drug treatment (A375), and three multi-day, large-scale movies with up to five mitoses per lineage (MCF10A, A375, and RPE-hTERT) ([STAR Methods](#); [Table S2](#)). We benchmarked the cell trackers on six criteria ([STAR Methods](#)). Two criteria were adopted from the Cell Tracking Challenge: SEG, a measure of segmentation quality based on the pixel match (Jaccard similarity index) between segmented nuclei and manual annotation; and TRA, a measure of tracking accuracy based on the similarity (normalized acyclic-oriented graph-matching measure) between identified cell lineages and manual annotation. We also included four criteria from the perspective of biologists: %CORR\_S, the percentage of cell nuclei that were correctly segmented before track linking, as evaluated by manual inspection; #COMP, the number of complete tracks in which cells were continuously tracked throughout the movie; #MIS\_T, the average number of mistakes among the complete tracks; and %CORR\_T, the percentage of complete tracks that were correctly tracked.

Benchmarked results are summarized in [Table 1](#). For segmentation, EllipTrack did not achieve a high pixel match with the manual annotation (low SEG score) because of the approximate nature of ellipse fitting, although it correctly segmented most cells in the movies, as evidenced by top scores for %CORR\_S. This result suggests that EllipTrack is suitable for biological research in which cells are hard to identify and the identification of perfect nuclear contours is not absolutely necessary. For track linking, benchmarking shows that the local track-correction module of EllipTrack corrected a substantial number of tracking mistakes, such that the tracking results after correction achieved one of the top track-linking scores across almost all movies. The improvement was especially significant for the three large-scale datasets in which cells were more crowded. Other cell trackers may have higher scores in some criteria. For example, for the MCF10A movie (“MCF10A-1”), [Cappell et al. \(2016, 2018\)](#) tracked very few cells but with high accuracy, whereas BaxterAlgorithm and iLastik tracked more cells but made many more errors. However, the former would correspondingly have a very limited coverage of the diverse cell behaviors in the movie, whereas the latter two would require significant manual effort to correct mistakes before downstream analysis could be performed. In comparison, EllipTrack achieved a proper balance between coverage and accuracy because it obtained more than 70% of all possible complete tracks and more than half of the identified complete tracks were completely error free. Together, this benchmarking effort indicates that EllipTrack outperformed the other state-of-the-art cell trackers and demonstrates the power of the local track-correction module to obtain nearly error-free cell lineages.

**Table 1. Results of Cell Tracker Benchmark**

Movie (GT #COMP)	Cell Tracker	Segmentation		Track Linking			
		SEG	%CORR_S	TRA	#COMP	#MIS_T	%CORR_T
MCF10A-1 (453) large scale	EllipTrack w/ corr	0.7148	96*	0.9367*	324*	0.63*	55*
	EllipTrack w/o corr <sup>a</sup>	0.7168	96*	0.9336	105	7.68	1
	BaxterAlgorithm	0.8473*	97*	0.9311	383*	2.66	12
	Cappell et al. (2016, 2018)	0.8304*	93	0.9111	40	0.15*	90*
	iLastik	0.7758	88	0.9376*	457	2.25	23
A375-1 (281) large scale	EllipTrack w/ corr	0.6204	84*	0.9660*	140*	0.57*	61*
	EllipTrack w/o corr	0.6202	84*	0.9622	110	1.35	25
	BaxterAlgorithm	0.8619*	90*	0.9644	38	1.00	29
	Cappell et al. (2016, 2018)	0.7143	76	0.8353	34	0.88*	35*
	iLastik	0.7577*	50	0.9669*	254*	2.08	23
RPE-hTERT (60) large scale	EllipTrack w/ corr	0.6575	93*	0.9382*	15	3.80*	0
	EllipTrack w/o corr	0.6575	93*	0.9301*	19*	14.21	0
	BaxterAlgorithm	0.7845*	94*	0.9168	56*	7.55*	0
	Cappell et al. (2016, 2018)	0.7836	82	0.8720	0	N/A	N/A
	iLastik	0.8228*	65	0.9175	449	13.13	0
HeLa <sup>b</sup> (199.5)	EllipTrack w/ corr	0.7110	93*	0.9676*	189*	0.43*	66
	EllipTrack w/o corr	0.7172	93*	0.9669	185.5*	1.04	45
	BaxterAlgorithm <sup>c</sup>	0.8320*	93*	0.9821*	225	0.44	70*
	Cappell et al. (2016, 2018)	0.7001	73	0.8693	88.5	0.18*	85*
	iLastik	0.7574*	75	0.9639	253	1.33	40
BJ5TA (265)	EllipTrack w/ corr	0.7397	97*	0.9252	189*	0.03*	97
	EllipTrack w/o corr	0.7416	97*	0.9285*	186	0.03*	98*
	BaxterAlgorithm	0.7092	82	0.8027	201*	0.09	91
	Cappell et al. (2016, 2018)	0.7729*	89	0.8845	189*	0.01*	99*
	iLastik	0.7651*	91*	0.9363*	267	0.42	71

Good tracking performance is marked by a low #MIS\_T score and high scores for other criteria. For each criterion, the best and second-best scores are highlighted with an asterisk (\*). The three multi-day, large-scale movies are indicated with text “large-scale” under the “Movie” column. The ground-truth number of complete tracks (GT #COMP) was extracted from the manually annotated cell lineages and is shown under the Movie column. #COMP scores greater than the ground-truth value have a strike-through because the extra complete tracks must contain tracking mistakes. Abbreviations: w/, with; corr, correction; w/o, without; hTERT, human telomerase reverse transcriptase; N/A, not available.

<sup>a</sup>Because of a slightly different implementation of the Magnusson et al. (2015) global track-linking algorithm, EllipTrack without local track correction may perform worse than the BaxterAlgorithm. Refer to the STAR Methods for more information.

<sup>b</sup>Two HeLa movies were independently benchmarked, and the average results are shown.

<sup>c</sup>For HeLa movies, the parameter values provided with the BaxterAlgorithm were used. These values were fine tuned to maximize the SEG and TRA scores. Therefore, the tracking performance may be over-estimated.

### EllipTrack Can Infer Time- and Density-Dependent Cell Migration Speed

Cells often adjust their migration speed in response to environmental changes (Ridley et al., 2003). For example, examination of a typical cell in the previously mentioned MCF10A movie revealed a clear inverse relationship between the migration speed (the number of pixels traveled per frame) and the number of cells in the local neighborhood (Figure 2A). However, current cell trackers implementing the Magnusson et al. (2015) global track-linking algorithm assume a constant migration speed over the entire movie. When tracking the cell in Figure 2A, those cell trackers are likely to terminate the cell track prematurely and re-initiate a new one in the next frame in the region of low cell density because the probability for track termination and re-initiation is likely greater than the probability for migration of a cell

with an underestimated speed. Meanwhile, when the local density is high, those trackers may map the cell track to an incorrect neighboring cell. Consequently, the identified cell lineages will contain numerous mistakes.

To account for that variable cell behavior, EllipTrack implements an option to perform time- and local cell-density-dependent inference of cell migration speeds from the training datasets. Users can select the best option based on whether there exists a clear trend between the migration speeds and time/density values. As a demonstration, we performed a density-dependent inference (denoted as the “density” option) on the training datasets from the MC10A movie and indeed found a clear dependency between migration distances and local cell densities (Figure 2B, black line). In contrast, assuming a constant migration speed over time (denoted as the “global” option),

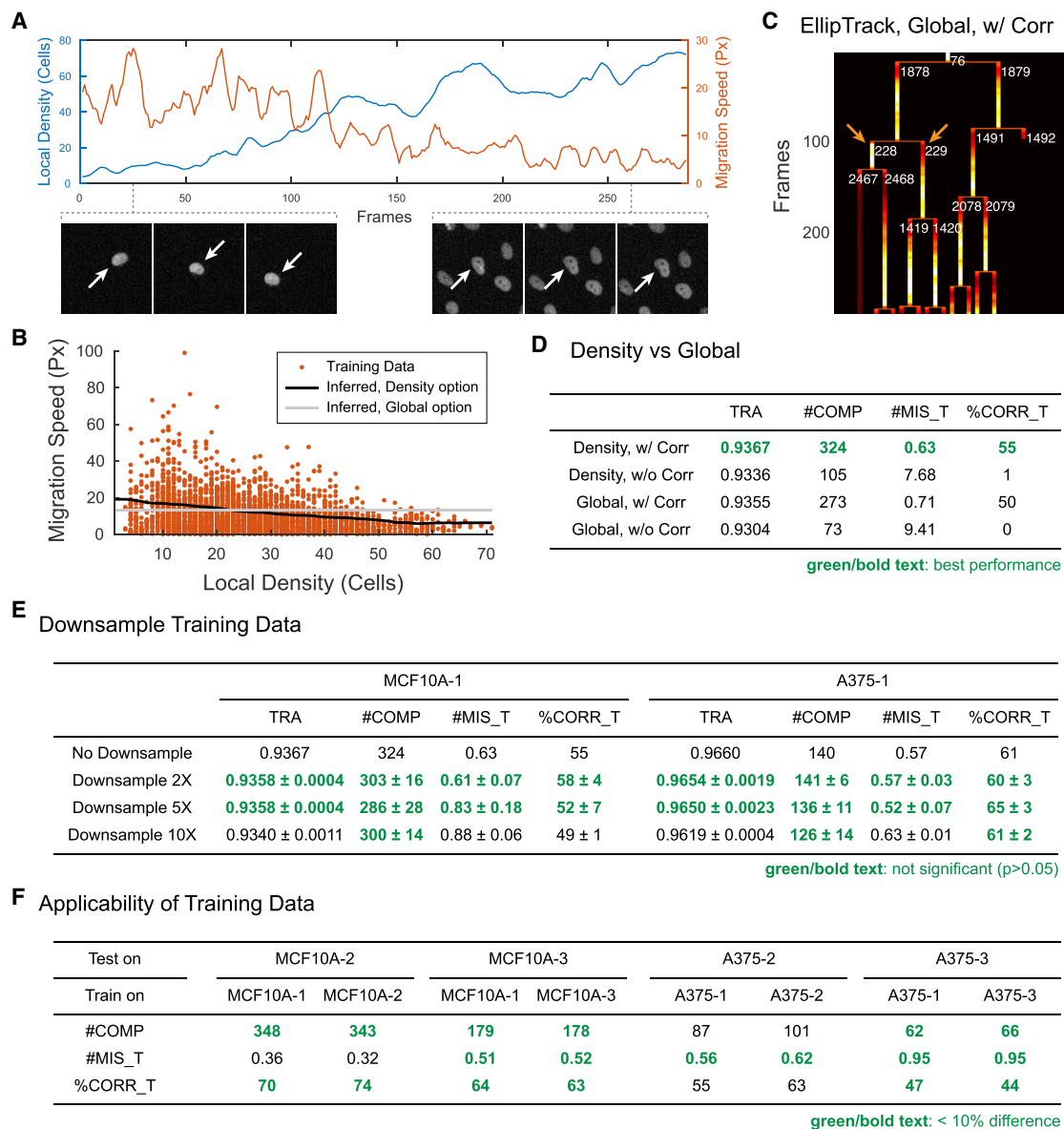


**Figure 2. Inference of Cell Migration Speeds and Characterization of Training Datasets**

(A) Cell migration speeds are density dependent. Top: comparison of migration speed (Euclidean distance per frame in pixels) and the number of cells in the local neighborhood at each frame for a single cell. Bottom: images of the cell at the sparsely (left) and densely (right) populated regions. Images from three consecutive frames are shown. White arrows indicate the cell plotted in the top panel. Dataset: MCF10A-1.

(B) Inference of cell migration speed from training datasets. Dots represent the migration of cells from one frame to the next: one dot is plotted for the number of pixels traveled in the x direction, and a second dot is plotted for the number of pixels traveled in the y direction. Black and gray lines indicate the inferred cell migration speeds with the “density” and “global” option, respectively. Dataset: MCF10A-1.

(C) Visualization of identified cell lineage, as in Figure 1F, but by EllipTrack with the “global” option.

(D) Comparison of the tracking performance between the “density” and “global” options. The highest score in each criterion is highlighted in bold green. Dataset: MCF10A-1. Scores of the density option are reproduced from Table 1.

(E) Relationship between the number of training samples and the tracking performance. Down-sampling was performed by randomly selecting a subset of the original training datasets. Means ± SD (n = 3) are shown for each down-sampling scheme. Scores that have no significant difference (p > 0.05, one-sided t test) from the “no down-sampling” scheme are highlighted in bold green. Scores without down-sampling are reproduced from Table 1.

(F) Applicability of training datasets to the tracking of untrained movies. Scores with less than 10% difference are highlighted in bold green.

inferred from the training datasets without consideration of time or density values, does not reflect the distribution of cell migration speeds (Figure 2B, gray line).

To demonstrate how the density option improves tracking performance, we tracked the MCF10A movie with both the density (used in the previous benchmark) and the global options.

Visualization of the same cell lineage in Figure 1F on CDK2-activity-based heatmaps revealed that the density option tracked the entire lineage without errors (Figure 1F), whereas the global option incorrectly swapped two cell tracks (Figure 2C). Furthermore, we systematically benchmarked those two options and found that the density option outperformed the global option in all track-linking criteria (Figure 2D). It is worth mentioning that even with the global option, half of the identified complete tracks were error free, which further demonstrates the power of the local track-correction module. In summary, the time- and density-dependent inference option complements the local track-correction module and allows users to achieve an even better tracking performance for appropriate movies.

### EllipTrack Requires Minimal Training

EllipTrack relies on user-provided training samples to construct cell tracks. A training sample describes a cell event (e.g., mitosis, apoptosis) or migration and can be constructed with a user-friendly graphical user interface (GUI) application with two mouse clicks (STAR Methods; Figure S2). When benchmarking the MCF10A and A375 movies, we constructed 2,922 and 2,136 samples for cell events, and labeled 37 and 55 cells for cell migration, respectively. To determine how many samples EllipTrack requires for accurate cell tracking, we down-sampled the training datasets to various degrees and examined the change in tracking performance. As shown in Figure 2E, EllipTrack displays a consistent performance when down-sampled 5-fold. With further down-sampling, tracking performance worsened and a marginally greater number of tracking errors occurred. This analysis suggests that creating ~500 training samples and labeling ~10 cells that are representative of cell events and migration are sufficient for high-accuracy tracking.

To determine whether training datasets from one movie could be used to track other movies, we created two additional movies of MCF10A (untreated) and A375 cells (treated with 1  $\mu$ M of dabrafenib) by imaging cells under identical conditions. We then compared the tracking performance using the previously generated training datasets versus using training datasets generated from the new movies. In all four movies, EllipTrack demonstrated comparable tracking in both scenarios (Figure 2F), indicating the good predictive power of the training datasets for tracking untrained movies of the same cell line under the same imaging conditions. This brings substantial time savings because each cell line only needs to be trained once.

### DISCUSSION

Time-lapse microscopy provides an unprecedented opportunity to observe single-cell dynamics in real time. However, existing computational tools often track cells with limited accuracy and extensive human labor can be required to correct cell tracks manually, both of which prevent efficient high-throughput monitoring of cells over long periods. This work describes EllipTrack, a new cell-tracking pipeline that combines the best features of previous segmentation and tracking algorithms and also implements a new local track-correction module to generate nearly error-free cell lineages. We also demonstrate EllipTrack's ability to perform a time- and density-dependent migration-speed infer-

ence and characterize the amount of training data required for successful tracking. EllipTrack offers two user-friendly GUI applications that allow users to set up parameter values and to create training datasets with minimal actions (STAR Methods; Figure S2). EllipTrack can be applied to address a wide range of biological questions and is especially suitable for drug screens and systems pharmacology because it can handle large-scale movies with time-dependent changes in migration that occur upon drug treatment. EllipTrack has already proved essential in two projects from our laboratory, enabling new discoveries about proliferation in both normal and cancer cells (Min et al., 2020; Yang et al., 2020).

Despite its better performance, EllipTrack has a few limitations. First, because of the comprehensiveness of local track correction, EllipTrack requires at least a 2-fold-longer run time compared with other benchmarked cell trackers, and it is often necessary to track multiple movies in parallel on a computing cluster. Second, cells with kidney-shaped or other non-elliptical nuclei are often over-segmented, although we find that signals can still be reliably extracted. Third, EllipTrack does not consider unusual cell behaviors, such as multipolar mitoses and cell-cell fusion, although those behaviors can be incorporated if needed. Similarly, whole-cell segmentation could also be incorporated via the use of whole-cell markers, if needed. In summary, EllipTrack extends our current capacity of tracking multi-day, large-scale movies, and the plethora of single-cell traces identified by EllipTrack can accelerate the discovery of heterogeneous cell behaviors over long periods.

### STAR★METHODS

Detailed methods are provided in the online version of this paper and include the following:

- KEY RESOURCES TABLE
- RESOURCE AVAILABILITY
  - Lead Contact
  - Materials Availability
  - Data and Code Availability
- EXPERIMENTAL MODEL AND SUBJECT DETAILS
  - Cell Lines
- METHOD DETAILS
  - Time-Lapse Microscopy
  - Implementation of EllipTrack
  - Graphical User Interfaces
  - Description of Movies
  - Benchmarking Criteria
  - Parameters used for Benchmarking
- QUANTIFICATION AND STATISTICAL ANALYSIS

### SUPPLEMENTAL INFORMATION

Supplemental Information can be found online at <https://doi.org/10.1016/j.celrep.2020.107984>.

### ACKNOWLEDGMENTS

We thank the members of the Spencer Lab for general help. This work was primarily supported by a Beckman Young Investigator award to S.L.S. and in part



by a Kimmel Scholar award (SKF16-126) and a Searle Scholar Program award (SSP-2016-1533) to S.L.S.

#### AUTHOR CONTRIBUTIONS

C.T. and C.Y. designed, conducted, and analyzed the experiments. C.T. developed and tested EllipTrack. S.L.S. conceived the project, suggested the experiments, and interpreted the data. C.T. and S.L.S. wrote the manuscript.

#### DECLARATION OF INTERESTS

The authors declare no competing interests.

Received: July 5, 2019

Revised: May 29, 2020

Accepted: July 9, 2020

Published: August 4, 2020

#### REFERENCES

- Amat, F., Lemon, W., Mossing, D.P., McDole, K., Wan, Y., Branson, K., Myers, E.W., and Keller, P.J. (2014). Fast, accurate reconstruction of cell lineages from large-scale fluorescence microscopy data. *Nat. Methods* *11*, 951–958.
- Arbelle, A., Reyes, J., Chen, J.Y., Lahav, G., and Riklin Raviv, T. (2018). A probabilistic approach to joint cell tracking and segmentation in high-throughput microscopy videos. *Med. Image Anal.* *47*, 140–152.
- Arora, M., Moser, J., Phadke, H., Basha, A.A., and Spencer, S.L. (2017). Endogenous replication stress in mother cells leads to quiescence of daughter cells. *Cell Rep.* *19*, 1351–1364.
- Berg, S., Kutra, D., Kroeger, T., Straehle, C.N., Kausler, B.X., Haubold, C., Schiegg, M., Ales, J., Beier, T., Rudy, M., et al. (2019). ilastik: interactive machine learning for (bio)image analysis. *Nat. Methods* *16*, 1226–1232.
- Cappell, S.D., Chung, M., Jaimovich, A., Spencer, S.L., and Meyer, T. (2016). Irreversible APC/Cdh1 Inactivation Underlies the Point of No Return for Cell-Cycle Entry. *Cell* *166*, 167–180.
- Cappell, S.D., Mark, K.G., Garbett, D., Pack, L.R., Rape, M., and Meyer, T. (2018). EMI1 switches from being a substrate to an inhibitor of APC/C<sup>CDH1</sup> to start the cell cycle. *Nature* *558*, 313–317.
- Chung, M., Liu, C., Yang, H.W., Koberlin, M.S., Cappell, S.D., and Meyer, T. (2019). Transient hysteresis in CDK4/6 activity underlies passage of the restriction point in G1. *Mol. Cell* *76*, 562–573.e564.
- Cooper, S., Barr, A.R., Glen, R., and Bakal, C. (2017). NucliTrack: an integrated nuclei tracking application. *Bioinformatics* *33*, 3320–3322.
- Gillies, T.E., Pargett, M., Minguet, M., Davies, A.E., and Albeck, J.G. (2017). Linear integration of ERK activity predominates over persistence detection in Fra-1 regulation. *Cell Syst.* *5*, 549–563.e545.
- Gookin, S., Min, M., Phadke, H., Chung, M., Moser, J., Miller, I., Carter, D., and Spencer, S.L. (2017). A map of protein dynamics during cell-cycle progression and cell-cycle exit. *PLoS Biol.* *15*, e2003268.
- Han, H., Wu, G., Li, Y., and Zi, Z. (2019). eDetect: a fast error detection and correction tool for live cell imaging data analysis. *iScience* *13*, 1–8.
- He, T., Mao, H., Guo, J.X., and Yi, Z. (2017). Cell tracking using deep neural networks with multi-task learning. *Image Vis. Comput.* *60*, 142–153.
- Hernandez, D.E., Chen, S.W., Hunter, E.E., Steager, E.B., and Kumar, V. (2018). Cell tracking with deep learning and the viterbi algorithm. In *Proceedings of the 2018 International Conference on Manipulation, Automation and Robotics at Small Scales*, S. Haliyo, A. Sill, F. Arai, and S. Fatikow, eds. (MARSS), pp. 1–6.
- Hilsenbeck, O., Schwarzfischer, M., Skylaki, S., Schaubberger, B., Hoppe, P.S., Loeffler, D., Kokkalis, K.D., Hastreiter, S., Skylaki, E., Filipczyk, A., et al. (2016). Software tools for single-cell tracking and quantification of cellular and molecular properties. *Nat. Biotechnol.* *34*, 703–706.
- Kudo, T., Jeknić, S., Macklin, D.N., Akhter, S., Hughey, J.J., Regot, S., and Covert, M.W. (2018). Live-cell measurements of kinase activity in single cells using translocation reporters. *Nat. Protoc.* *13*, 155–169.
- Magnusson, K.E.G., Jalden, J., Gilbert, P.M., and Blau, H.M. (2015). Global linking of cell tracks using the Viterbi algorithm. *IEEE Trans. Med. Imaging* *34*, 911–929.
- Maška, M., Ulman, V., Svoboda, D., Matula, P., Matula, P., Ederra, C., Urbiola, A., España, T., Venkatesan, S., Balak, D.M., et al. (2014). A benchmark for comparison of cell tracking algorithms. *Bioinformatics* *30*, 1609–1617.
- Min, M., Rong, Y., Tian, C., and Spencer, S.L. (2020). Temporal integration of mitogen history in mother cells controls proliferation of daughter cells. *Science* *368*, 1261–1265.
- Moen, E., Borba, E., Miller, G., Schwartz, M., Bannon, D., Koe, N., Camplisson, I., Kyme, D., Pavelchek, C., Price, T., et al. (2019). Accurate cell tracking and lineage construction in live-cell imaging experiments with deep learning. *bioRxiv*. <https://doi.org/10.1101/803205>.
- Ridley, A.J., Schwartz, M.A., Burridge, K., Firtel, R.A., Ginsberg, M.H., Borisy, G., Parsons, J.T., and Horwitz, A.R. (2003). Cell migration: integrating signals from front to back. *Science* *302*, 1704–1709.
- Sakaue-Sawano, A., Kurokawa, H., Morimura, T., Hanyu, A., Hama, H., Osawa, H., Kashiwagi, S., Fukami, K., Miyata, T., Miyoshi, H., et al. (2008). Visualizing spatiotemporal dynamics of multicellular cell-cycle progression. *Cell* *132*, 487–498.
- Skylaki, S., Hilsenbeck, O., and Schroeder, T. (2016). Challenges in long-term imaging and quantification of single-cell dynamics. *Nat. Biotechnol.* *34*, 1137–1144.
- Sommer, C., Straehle, C., Kothe, U., and Hamprecht, F.A. (2011). Ilastik: interactive learning and segmentation toolkit. In *Proceedings of the IEEE International Symposium on Biomedical Imaging: From Nano to Macro*, S. Wright, X. Pan, and M. Liebling, eds., pp. 230–233.
- Spencer, S.L., Cappell, S.D., Tsai, F.C., Overton, K.W., Wang, C.L., and Meyer, T. (2013). The proliferation-quiescence decision is controlled by a bifurcation in CDK2 activity at mitotic exit. *Cell* *155*, 369–383.
- Turetken, E., Wang, X., Becker, C.J., Haubold, C., and Fua, P. (2017). Network flow integer programming to track elliptical cells in time-lapse sequences. *IEEE Trans. Med. Imaging* *36*, 942–951.
- Ulman, V., Maška, M., Magnusson, K.E.G., Ronneberger, O., Haubold, C., Harder, N., Matula, P., Matula, P., Svoboda, D., Radojevic, M., et al. (2017). An objective comparison of cell-tracking algorithms. *Nat. Methods* *14*, 1141–1152.
- Wolff, S.C., Kedziora, K.M., Dumitru, R., Dungee, C.D., Zikry, T.M., Beltran, A.S., Haggerty, R.A., Cheng, J., Redick, M.A., and Purvis, J.E. (2018). Inheritance of OCT4 predetermines fate choice in human embryonic stem cells. *Mol. Syst. Biol.* *14*, e8140.
- Yang, C., Tian, C., Hoffman, T.E., Jacobsen, N.K., and Spencer, S.L. (2020). Rapidly induced drug adaptation mediates escape from BRAF inhibition in single melanoma cells. *bioRxiv*. <https://doi.org/10.1101/2020.03.15.992982>.
- Yu, D., Baird, M.A., Allen, J.R., Howe, E.S., Klassen, M.P., Reade, A., Makhijani, K., Song, Y., Liu, S., Murthy, Z., et al. (2015). A naturally monomeric infrared fluorescent protein for protein labeling in vivo. *Nat. Methods* *12*, 763–765.
- Zafari, S., Eerola, T., Sampo, J., Kälviäinen, H., and Haario, H. (2015). Segmentation of overlapping elliptical objects in silhouette images. *IEEE Trans. Image Process.* *24*, 5942–5952.

## STAR★METHODS

### KEY RESOURCES TABLE

REAGENT or RESOURCE	SOURCE	IDENTIFIER
Chemicals, Peptides, and Recombinant Proteins		
Dabrafenib (GSK2118436)	Selleckchem	Cat#S2807
Sodium Bicarbonate	Fisher Chemical	Cat#S233-500
DMEM Phenol red free	Corning	Cat#90-013-PB
DMEM/F12 Phenol red free	Thermo Fisher	Cat#11330-021
Horse Serum	Thermo Fisher	Cat#16050-122
Epidermal Growth Factor	Peptotech	Cat#AF-100-15
Hydrocortisone	Sigma	Cat#H0888-1g
Insulin	Sigma	Cat#I1882-200mg
Cholera Toxin	Sigma	Cat#C8052-2mg
PBS	Thermo Fisher	Cat#14190-144
Collagen	Advanced BioMatrix	Cat#5005-100ML
Deposited Data		
Raw and analyzed data	This manuscript	<a href="https://drive.google.com/drive/folders/1dEW-cDlwZLrgA-yPLjuB2Ok2DhV2qQS">https://drive.google.com/drive/folders/1dEW-cDlwZLrgA-yPLjuB2Ok2DhV2qQS</a>
Experimental Models: Cell Lines		
A375 cell line	ATCC	Cat# CRL-1619, RRID:CVCL_0132
A375 H2B-mIFP DHB-mCherry, FIRE-mVenus	This manuscript	N/A
MCF10A H2B-mTurquoise, DHB-mCherry, endogenously tagged mCitrine-Cyclin D1	(Gookin et al., 2017)	N/A
Software and Algorithms		
MATLAB	Mathworks	R2017a-R2019b
EllipTrack	This manuscript	<a href="https://github.com/tianchengzhe/elliptrack">https://github.com/tianchengzhe/elliptrack</a>
Other		
96 well glass bottom plate	Cellvis	Cat# P96-1.5H-N

### RESOURCE AVAILABILITY

#### Lead Contact

Further information and requests for resources and reagents should be directed to and will be fulfilled by the Lead Contact, Sabrina Leigh Spencer ([sabrina.spencer@colorado.edu](mailto:sabrina.spencer@colorado.edu)).

#### Materials Availability

The cell lines generated in this study are available upon request.

#### Data and Code Availability

EllipTrack is available at <https://github.com/tianchengzhe/EllipTrack>. Documentation is available at <https://elliptrack.readthedocs.io/en/latest/>. Scripts and movies used in this study are available upon request.

### EXPERIMENTAL MODEL AND SUBJECT DETAILS

#### Cell Lines

MCF10A human mammary epithelial cells were obtained from Gookin et al. (2017) and maintained in DMEM/F12 supplemented with 5% horse serum, 20ng/mL epidermal growth factor, 0.5 mg/mL hydrocortisone, 100ng/mL cholera toxin, 10 µg/mL insulin, and 1X penicillin/streptomycin. A375 melanoma cells were purchased from the American Type Culture Collection, transduced with H2B-mIFP (Yu et al., 2015), DHB-mCherry (Spencer et al., 2013), and FIRE-mVenus (Gillies et al., 2017) lentivirus, and were maintained

in DMEM supplemented with 10% FBS, 1.5g/L sodium bicarbonate and 1X penicillin/streptomycin. Both cell lines were cultured at 37°C in a 5% CO<sub>2</sub> humidified incubator.

## METHOD DETAILS

### Time-Lapse Microscopy

Time-lapse microscopy was performed as previously described (Arora et al., 2017). In brief, cells were plated on a 96-well plate coated with collagen (1:50 dilution in water) in phenol red-free full growth medium. Approximately 24 hr later, cells were transferred to a Ti-E PFS (Nikon) with a humidified, 37°C chamber with 5% CO<sub>2</sub>, and imaged periodically with a 10X 0.45 NA objective. Drug was added to the medium by pausing the movie, exchanging 50% of the medium in the well with medium containing 2X drug concentration, and restarting the movie. Movie-specific parameters are described below.

#### A375 Movie

A375 cells expressing H2B-mIFP (Yu et al., 2015), DHB-mCherry, and FIRE-mVenus were plated with a density of 1000 cells/well. Images were taken every 15 min with the following exposure times: mIFP 300 ms, mCherry 50 ms, and YFP 100 ms. Data from the mCherry and YFP channels was not used in this study. Cells were first imaged in full growth medium for 24 hr (96 frames). The BRAF inhibitor dabrafenib was then added to the well as described above and cells were imaged for a further 96.5 hr (386 frames). Drug was refreshed 30 hr after drug addition.

#### MCF10A Movie

MCF10A cells expressing H2B-mTurquoise, DHB-mCherry, and endogenously tagged mCitrine-Cyclin D1 (Gookin et al., 2017) were plated with a density of 1000 cells/well and cultured in full growth medium. Cells were imaged every 10 min for 48 hr (288 frames) with the following exposure times: CFP 20 ms, and mCherry 100 ms. The YFP channel was not imaged.

### Implementation of EllipTrack

A schematic diagram of EllipTrack is shown in Figure S1A. In brief, EllipTrack first segments the cell nuclei in the images of the nuclear marker and fits them with ellipses (Segmentation). Then, displacement between every two images in neighboring frames (called “jitters”) is calculated and the positional information of ellipses are corrected (Jitter Correction). Next, EllipTrack constructs cell tracks based on the ellipse information (Track Linking). Tracking results can be optionally visualized by creating the “vistrack” movies (Visualize Tracking). Finally, EllipTrack extracts signals from each ellipse and constructs time series for each cell track (Signal Extraction).

#### Segmentation

In Segmentation, an image of the nuclear channel is first background subtracted and binarized (“Image Binarization”) such that pixels within a nucleus are assigned a value of 1 (foreground pixels) and pixels in the image background are assigned a value of 0 (background pixels). The binary image is then optimized by the active contour (“Active Contour”) and Watershed (“Watershed”) algorithms. Next, ellipses are fit to the contours of foreground pixels in the optimized binary image (“Ellipse Fitting”) and corrected with user-provided training datasets (“Correction with Training Datasets”). Finally, EllipTrack extracts features from each ellipse that will be used in Track Linking (“Feature Extraction”). “Image Binarization,” “Ellipse Fitting,” and “Feature Extraction” are required.

In Image Binarization, two options are provided to binarize images: thresholding and blob detection. For thresholding, a threshold is applied to the intensities of the nuclear image. Pixels with intensities greater than the threshold are assigned as foreground pixels while other pixels are assigned as background pixels. For blob detection, the hessian matrix of the nuclear image is computed and a threshold is applied to the hessian matrix. Pixels with values less than the threshold are assigned as foreground pixels and other pixels are assigned as background pixels. A set of connected foreground pixels is called a component.

In Active Contour, the exact boundaries of components in the binary image are searched with the active contour algorithm. EllipTrack provides two options. The “global” option applies the active contour algorithm to the entire image, while the “local” option applies the algorithm to the local neighborhood of every component and the outputs from each local neighborhood are then assembled. The “global” option is computationally efficient, while the “local” option detects the boundaries more accurately, especially for dim nuclei.

In Watershed, multiple nuclei within a component are separated with the Watershed algorithm. To improve the robustness of the algorithm, the “peaks” of watershed are not defined by the pixels with local maximal distances to the background. Instead, they are defined by small components constructed by repeatedly eroding the binary image.

In Ellipse Fitting, contours of components in the binary image are fit with ellipses with a previously published algorithm (Zafari et al., 2015). In brief, the algorithm first searches for a characteristic point (called “seedpoint”) for each nucleus. The contours of components are then assigned to the seedpoints. Finally, the contour assigned to each seedpoint is fit with an ellipse.

In Correction with Training Datasets, EllipTrack constructs a linear discriminant classifier with user-provided training datasets (see “Construct Training Data” of “Track Linking”) and predicts the number of nuclei each ellipse contains. Ellipses with a high probability of containing no nucleus are removed, while ellipses with a high probability of containing two or more nuclei are split into two using the k-means algorithm. To ensure the robustness of splitting, two runs of the k-means algorithm are performed and the ellipse is only split if these two runs show a high level of agreement.

Finally in Feature Extraction, a predefined set of 26 features is extracted from each ellipse (Table S3). Features include the morphological parameters of the fitted ellipses and the distribution of nuclear marker intensities within the ellipses.

### Jitter Correction

EllipTrack offers two options to perform jitter correction: local and global. With the local option, EllipTrack computes the jitters between every two neighboring frames (called “local jitters”) by image registration (as in Cappell et al., 2016), and then corrects the positional information of ellipses by subtracting the jitters from their original positions on the images. Movies are corrected independently, even if they are captured on the same plate.

Meanwhile, for movies captured on the same multi-well plate, jitters are often correlated because they are subject to the same plate motion. It is therefore possible to infer the plate motion from this correlation and use it to compute the jitters for each movie based on its position on the plate, an approach that can significantly reduce the errors of calculation. EllipTrack implements this approach with the global option, where the plate motion between every two frames is inferred from the local jitters, and the jitters calculated from the plate motion (called “global jitters”) are then used to correct the positions of ellipses.

Mathematically: denote the position of well  $(i, j)$  in frame  $t$  as  $(x_{ij}^t, y_{ij}^t)$  and the distances between two rows and two columns as  $v$  and  $h$ , respectively, as below

$$(x_{ij}^t, y_{ij}^t) = (x_{1,1}^t, y_{1,1}^t) + ((j-1)h, (i-1)v)$$

Assume that the plate motion between frame  $t$  and frame  $t+1$  causes a whole-plate shift of  $(\Delta x, \Delta y)$  and a plate rotation of angle  $\theta$ . The position of well  $(i, j)$  in frame  $t+1$  can then be expressed as

$$(x_{ij}^{t+1}, y_{ij}^{t+1}) = (x_{1,1}^t, y_{1,1}^t) + (\Delta x, \Delta y) + \mathbf{R}((j-1)h, (i-1)v)$$

where  $\mathbf{R}$  is the rotation matrix for the angle  $\theta$ . Therefore, the motion of the well (i.e., global jitters) follows

$$(\Delta x_{ij}^{t+1}, \Delta y_{ij}^{t+1}) = (x_{ij}^{t+1}, y_{ij}^{t+1}) - (x_{ij}^t, y_{ij}^t) = (\Delta x, \Delta y) + (\mathbf{R} - \mathbf{I})((j-1)h, (i-1)v) \quad (1)$$

with  $\mathbf{I}$  being the identity matrix. Local jitters inferred by image registration are equal to the sum of the global jitters and the error terms, as shown below.

$$(\Delta \tilde{x}_{ij}^{t+1}, \Delta \tilde{y}_{ij}^{t+1}) = (\Delta x_{ij}^{t+1}, \Delta y_{ij}^{t+1}) + (\epsilon_x, \epsilon_y), \text{ where } \epsilon_x \text{ and } \epsilon_y \sim N(0, \sigma^2)$$

EllipTrack uses the local jitters  $(\Delta \tilde{x}_{ij}^{t+1}, \Delta \tilde{y}_{ij}^{t+1})$  and the position  $(i, j)$  of each well to infer the unknown variables  $(h, v, \theta, \Delta x, \Delta y)$  and then computes the global jitters of each well with Equation 1.

### Track Linking

In Track Linking, users first create training datasets with the Training Data Generator GUI attached to EllipTrack (“Construct Training Data”) and EllipTrack uses these datasets to predict the behaviors of each ellipse in the movie (“Compute Probabilities”). Cell tracks are then generated based on these predictions (“Construct Tracks”). Finally, errors in cell tracks are fixed by the local track-correction module (“Local Track Correction”).

In Construct Training Data, users load ellipse information into the GUI attached to EllipTrack and manually label the behavior (called “events”) of each ellipse. Two types of events are considered: morphological events and motion events. Morphological events describe the status and behavior of the ellipse in the current frame and include the number of cell nuclei in the ellipse (0, 1, or 2) as well as whether cells are mitotic, newly born, or apoptotic. Motion events describe cell migration between neighboring frames and include migration between two ellipses in neighboring frames and migration in/out of the field of view. Motion events are also used to infer the migration speed of cells. After users label all events of interest, the GUI generates a training dataset which can be used for computing probabilities.

In Compute Probabilities, EllipTrack constructs linear discriminant classifiers with user-provided training datasets and computes the probabilities of morphological events for each ellipse. For motion events, EllipTrack models cell migration by random walk (as in Magnusson et al., 2015), and calculates the probabilities of cell migration with the formula

$$P(D_{i,t} \rightarrow D_{j,t+1}) = \frac{P_{sim}(D_{i,t}, D_{j,t+1})p_{mig}(D_{i,t}, D_{j,t+1})}{P_{sim}(D_{i,t}, D_{j,t+1})p_{mig}(D_{i,t}, D_{j,t+1}) + [1 - P_{sim}(D_{i,t}, D_{j,t+1})]p_{nonmig}}$$

Here,  $D_{i,t}$  and  $D_{j,t+1}$  refers to the  $i$ -th ellipse in Frame  $t$  and  $j$ -th ellipse in Frame  $t+1$ ;  $P_{sim}(D_{i,t}, D_{j,t+1})$  refers to the probability that these two ellipses represent the same cell, as predicted by the linear discriminant classifiers constructed from the training datasets;  $p_{mig}(D_{i,t}, D_{j,t+1})$  refers to the probability that the cell migrates from the position of  $D_{i,t}$  to the position of  $D_{j,t+1}$ , as computed by the formula of random walk; and  $p_{nonmig}$  refers to the null probability of cell migration (a user-controlled parameter). A key parameter of a random walk is the standard deviation (i.e., cell migration speed). EllipTrack offers three options to compute this parameter: global, time, and density. With the global option, EllipTrack uses all training samples and infers a single migration speed for all cells in all frames. With the other two options, EllipTrack calculates the migration distances and the Frame ID (time) or the number of cells in the local neighborhood (density) for each training sample, and estimates the curve of migration speed versus

time/density from these samples. EllipTrack will then apply this curve to the movie and calculate the migration speed for each cell at each frame.

In Construct Tracks, EllipTrack uses the [Magnusson et al. \(2015\)](#) global track-linking algorithm to construct cell tracks. Note that in EllipTrack, the Magnusson swap operation only applies to the cell tracks that map to cells at both frames. Cell tracks that map to cells at only one frame at the frames of interest, such as those associated with appearance, disappearance, mitosis, and apoptosis, are not considered. In comparison, all cell tracks can be swapped in BaxterAlgorithm. Therefore, BaxterAlgorithm may show a better performance compared to EllipTrack before local track-correction ([Table 1](#)). However, all these overlooked mistakes can be fixed by the local track-correction module, and the tracking performance of EllipTrack after correction often becomes much better than BaxterAlgorithm.

Finally, in Local Track Correction, EllipTrack employs a six-step procedure to correct possible tracking mistakes. In the first step, EllipTrack optimizes the Magnusson swap operation and examines alternative track configurations, as described in the main text.

In the second step, EllipTrack corrects premature termination of cell tracks due to under- and over-segmentation. In the first case, when two cells are under-segmented by one ellipse and the predicted probabilities of cell overlap are not perfect, one cell might lose its cell track at the frame of under-segmentation and later be mapped by a new cell track at the frame where segmentation becomes correct. To fix this type of mistake, EllipTrack examines every pair of prematurely terminated cell track and newly created one, and will connect them if they meet the following requirements: (1) the latter cell track appears at most ‘track\_para.critical\_length’ (a user-controlled parameter) frames later than the termination of the former cell track, (2) both cell tracks share the same cell as their closest neighbor, and (3) the latter cell track does not appear by a mitosis event. In the second case, when one cell is over-segmented by two ellipses, its cell track might map to one of the two ellipses and terminates, while another cell track appears, maps to the other ellipse, and continues mapping this cell after segmentation becomes correct. To fix this type of mistake, EllipTrack examines every pair of prematurely terminated cell track and newly created one, and will combine them if they meet the following requirements: (1) the latter cell track appears at most ‘track\_para.critical\_length’ frames earlier than the termination of the former cell track, (2) both cell tracks are the closest neighbor of each other, and (3) the former cell track does not terminate by a mitosis event.

In the third step, EllipTrack corrects mistakes associated with under-segmentation. Due to its memoryless nature, the Magnusson global track-linking algorithm loses the identities of the cells when two cells are under-segmented and both cell tracks map to the same ellipse. Consequently, the algorithm randomly maps the cell tracks when cells are no longer under-segmented, which results in 50% of such mappings being incorrect. To correct these mistakes, EllipTrack compares the ellipse similarity and migration distances before and after under-segmentation and swaps the two cell tracks after under-segmentation if both quantities improve.

In the fourth step, EllipTrack searches for undetected mitosis events, which are marked by a cell track mapping both the mother cell and one daughter cell, and a second cell track mapping the other daughter cell. To do so, EllipTrack looks for all cell tracks which are not created by mitosis but have high probabilities of being a newly born cell at their first frame (as predicted in “Compute Probabilities”). For each cell track, EllipTrack then examines whether there exists a neighboring cell track that has a high probability of being a mitotic cell in the previous frame and has a high probability of being a newly born cell in the current frame. If such a cell track is found, EllipTrack will split the mother-and-daughter cell track into two (one for the mother cell, and the other for the daughter cell) and create a mitosis event between the mother cell track and the two daughter cell tracks.

In the fifth step, EllipTrack prunes the cell lineage trees by removing all cell tracks unlikely to represent a cell, such as very short cell tracks and cell tracks skipping too many frames. Mitosis events associated with these invalid cell tracks will be removed as well.

In the last step, EllipTrack recursively adjusts the Track IDs such that (1) Track IDs will be sorted by the ellipse positions at the first frame, and (2) sibling cells (two cells born by the same mother) have consecutive Track IDs. This step significantly reduces the mental burden when examining the “vistrack” movies.

### Visualize Tracking

To visualize the cell tracks, EllipTrack generates “vistrack” movies as in [Figure 1D](#).

### Signal Extraction

In Signal Extraction, EllipTrack defines the regions of nucleus and cytoplasmic ring for each ellipse as illustrated in [Figure S1C](#) and removes a pixel from the region if it is shared by other regions or cells ([Figure S1D](#)). EllipTrack then performs background subtraction on each fluorescent image, drops the outlier intensities (defined as the top and bottom 5%), and computes the mean, median, and variance of signal intensities in each region of each ellipse. Finally, the signal time series in each cell track are assembled for plotting.

### Graphical User Interfaces

To improve the practical usability of EllipTrack, we developed two user-friendly Graphical User Interfaces (GUIs), Parameter Generator GUI and Training Data GUI, to help users set up parameter values and construct training datasets ([Figure S2](#)). In Parameter Generator GUI, we classified parameters into two categories: basic and advanced. For most movies, setting the basic parameters is sufficient. We allow users to view the results of segmentation and migration-speed inference in real-time, thus providing a convenient parameter-tuning process. We also implement substantial hints and sanity-checks to prevent users from setting invalid values. In Training Data GUI, we simplify the training process such that creating a training sample involves only two mouse clicks and takes a few seconds. This allows users to generate the required ~500 training samples within 1 hr. Together, we expect that these GUIs help users to become familiar with EllipTrack in a short amount of time.

### Description of Movies

Movie statistics were summarized in Table S2. A detection refers to one nucleus in one frame. Based on the total number of detections, we classified MCF10A, A375, and RPE-hTERT movies as large-scale.

#### HeLa

Training movies of the Fluo-N2DL-HeLa dataset from the Cell Tracking Challenge. In each movie, HeLa cells expressing H2B-GFP were imaged every 30 min for 46 hr (92 frames) (Maška et al., 2014; Ulman et al., 2017). Official ground truth was used. These movies were among the most challenging datasets from the Cell Tracking Challenge.

#### BJ5TA

Courtesy of Steven Cappell. BJ5TA cells expressing H2B-mTurquoise and Geminin-mCherry (Sakaue-Sawano et al., 2008) were treated with control siRNA and then imaged every 12 min for ~20 hr (107 frames) (Cappell et al., 2016). Movie jitters were not corrected. 800 cell nuclei from four frames (Frame 23, 44, 81, 105) were annotated for segmentation benchmark and all cell lineages were annotated for tracking benchmark. The main difficulties include a drastic change of image background due to photobleaching, strong illumination bias, heterogeneous brightness of nuclei, and interference from other channels.

#### MCF10A

This movie was generated in this study. Experimental details were described above. Movie jitters were not corrected. 802 cells from four frames (Frame 41, 133, 217, 273) and all the cell lineages that present in the first frame were annotated. The main difficulties include rapid cell migration and dense cell distribution.

#### A375

This movie was generated in this study. Experimental details were described above. Movie jitters were corrected by BaxterAlgorithm. 668 cells from six frames (Frame 57, 106, 201, 210, 318, 480) and all cell lineages were annotated. The main difficulties include a drastic change of image background due to photobleaching, as well as abnormal cell morphology and strong overlap after drug treatment. Best efforts were made to annotate overlapping cells, though multiple cell lineages were not annotated to the end of the movie due to severe overlapping.

#### RPE-hTERT

Courtesy of Tammy Riklin Raviv and Jose Reyes. RPE-hTERT cells expressing H2B-mTurquoise, DDX5-eYFP, and p21-mVenus were imaged every 15 min for 100 hr (400 frames). Medium was refreshed at Frame 92, 181, 282, and 374 (Arbelle et al., 2018). Movie jitters were not corrected. For segmentation benchmark, manual annotation from Arbelle et al. were used (502 cells, from Frame 1, 20, 40, 60, 61, 80, 100, 190). For tracking benchmark, additional annotation was provided such that the majority of cell lineages, including all lineages that present in the first frame, were annotated. Main difficulties include strong cell overlap, rapid cell migration and dense cell distribution.

### Benchmarking Criteria

#### Cell Tracking Challenge Criteria (SEG and TRA)

These criteria evaluate the resemblance between tracking results and manually annotated ground truth. Ground truth was obtained as described above. Official evaluation programs were used to compute the scores. Since EllipTrack and Cappell et al. (2016, 2018) do not perform post-tracking segmentation, multiple cell tracks might map to the same nuclei, which is incompatible with the official evaluation programs. We therefore partitioned all such under-segmented nuclei with k-means algorithm and assigned track IDs based on the positions of nuclear centroids.

#### Accuracy of Segmentation (%CORR\_S)

This criterion examines whether cell nuclei are accurately segmented, without post-tracking segmentation. All cells from five equidistant frames spanning over the entire movie were examined (> 500 cells). Every cell nucleus was manually classified into four categories: correctly segmented, under-segmented (contains more than one nucleus), over-segmented (contains less than one nucleus), and not segmented. The percentage of nuclei that were correctly segmented was reported.

#### Number of Complete Tracks (#COMP)

This criterion examines the ability of cell trackers to track cells over long time periods. A complete track refers to a cell being tracked along the lineage tree from the first to the last frame of the movie. Cells migrating in/out of the field of view are excluded, regardless of whether they are correctly tracked or not. Ground truth of #COMP was derived from the manually annotated cell lineages.

#### Accuracy of Complete Tracks (#MIS\_T and %CORR\_T)

These criteria examine the ability of cell trackers to generate error-free cell tracks. Every complete track was manually examined and all tracking mistakes were annotated. A tracking mistake includes incorrect mapping between frames, incorrectly assigned mitosis events, and undetected mitosis events, but does not include mistakes due to segmentation. The average number of tracking mistakes in the complete tracks was reported as #MIS\_T, and the percentage of complete tracks that have no tracking mistakes was reported as %CORR\_T.

### Parameters used for Benchmarking

Parameter files of EllipTrack, BaxterAlgorithm, and Cappell et al. can be accessed at <https://drive.google.com/drive/folders/1dEW-cDlwZLrgA-yPLjuB2Ok2DHV2qQS>. iLastik files are available upon request.

### **EllipTrack**

For segmentation, parameters were tuned in Parameter Generator GUI such that cells from all frames were generally well-segmented. In brief, images were first background subtracted (HeLa only), log-transformed, and binarized (MCF10A and RPE-hTERT: thresholding, others: blob detection). Components in the binary images were then optimized with Active Contour (all but A375: log-transforming the raw images, all with the local option) and partitioned with Watershed. Finally, ellipse fitting was performed to the boundaries of components with the default parameters. For Track Linking, density-dependent migration speed inference was used for MCF10A and RPE-hTERT, while the global option was used for other movies. Default parameter values were used, except HeLa and A375 movies where some advanced parameters were tuned to improve the detection of mitosis events.

### **BaxterAlgorithm**

Parameters provided in BaxterAlgorithm were used to track the HeLa movies. For all other movies, the HeLa-movie parameters were imported and their values were then modified as follows. For Segmentation, the parameter 'BPSThreshold' was fine-tuned to achieve a good segmentation performance. Additional parameters, such as 'SegMinArea', might also be tuned to remove invalid components. For Track Linking, 'pDeath', 'TrackPAppear', 'TrackPDisappear', and 'TrackNumNeighbors' were modified to the same values as EllipTrack, and 'TrackXSpeedStd' was modified to the inferred migration speed by EllipTrack with the Global option. 'pCnt0', 'pCnt1', and 'pCnt2' were set to approximately match the proportions of over-, correctly, and under-segmented cells. Three parameters were tested with multiple values: 'TrackMaxMigScore' (0 or Inf), 'TrackMigLogLikeList' ('MigLogLikeList\_uniformClutter', or 'MigLogLikeList\_viterbiPaper'), and count/split/death classifiers ('none' or the ones created by training a subset of movie images). Tracking results from all eight parameter combinations were evaluated by the Cell Tracking Challenge evaluation software, and the combination with the highest (SEG+TRA)/2 score was used for benchmark.

### **Cappell et al., 2016, 2018**

Parameters related to movie specification, such as magnification of objective lens and average nuclear radius, were modified to match the experiments. Three parameter combinations were tested based on how the first and later frames were segmented: (1) the first frame with the 'log' option while later frames with the 'apriori' option; (2) the first frame with the 'single' option while later frames with the 'apriori' option; and (3) all frames with the 'log' option. The parameter combination with the highest (SEG+TRA)/2 score was used for benchmark.

### **iLastik**

For Segmentation, around 100 typical cells were selected from the entire movie. Pixels within the cell nuclei were trained as "Label 1" while the pixels immediately surrounding the nuclear contours were trained as "Label 2." Additionally, pixels from image background were trained as "Label 2." All features with the default standard deviation values were used for training. For Tracking, probabilities of segmentation were first smoothed with a sigma of 2x2, and then binarized with a threshold of 0.5. Components with area less than 25 (MCF10A) or 100 pixels (all other movies) were removed. Next, division and object count classifiers were trained on the same cells as EllipTrack. Training samples might be added or removed to avoid assertion errors. All features except locations were used for training. Finally, movies were tracked with the default parameters. Three values of border widths (HeLa, RPE-hTERT: 25, 50, 100 pixels, others: 50, 100, 200 pixels) were tested for each movie and the one with the highest (SEG+TRA)/2 score was used for benchmark.

## **QUANTIFICATION AND STATISTICAL ANALYSIS**

Data in [Figure 2E](#) are presented as mean  $\pm$  std; p value was derived from a one-sided t test. Sample number (n) represents the number of replicates. No other statistical analysis was performed in the study. Data analysis was not blinded.

**Cell Reports, Volume 32**

**Supplemental Information**

**EllipTrack: A Global-Local Cell-Tracking Pipeline  
for 2D Fluorescence Time-Lapse Microscopy**

**Chengzhe Tian, Chen Yang, and Sabrina L. Spencer**



**SUPPLEMENTAL FIGURES**

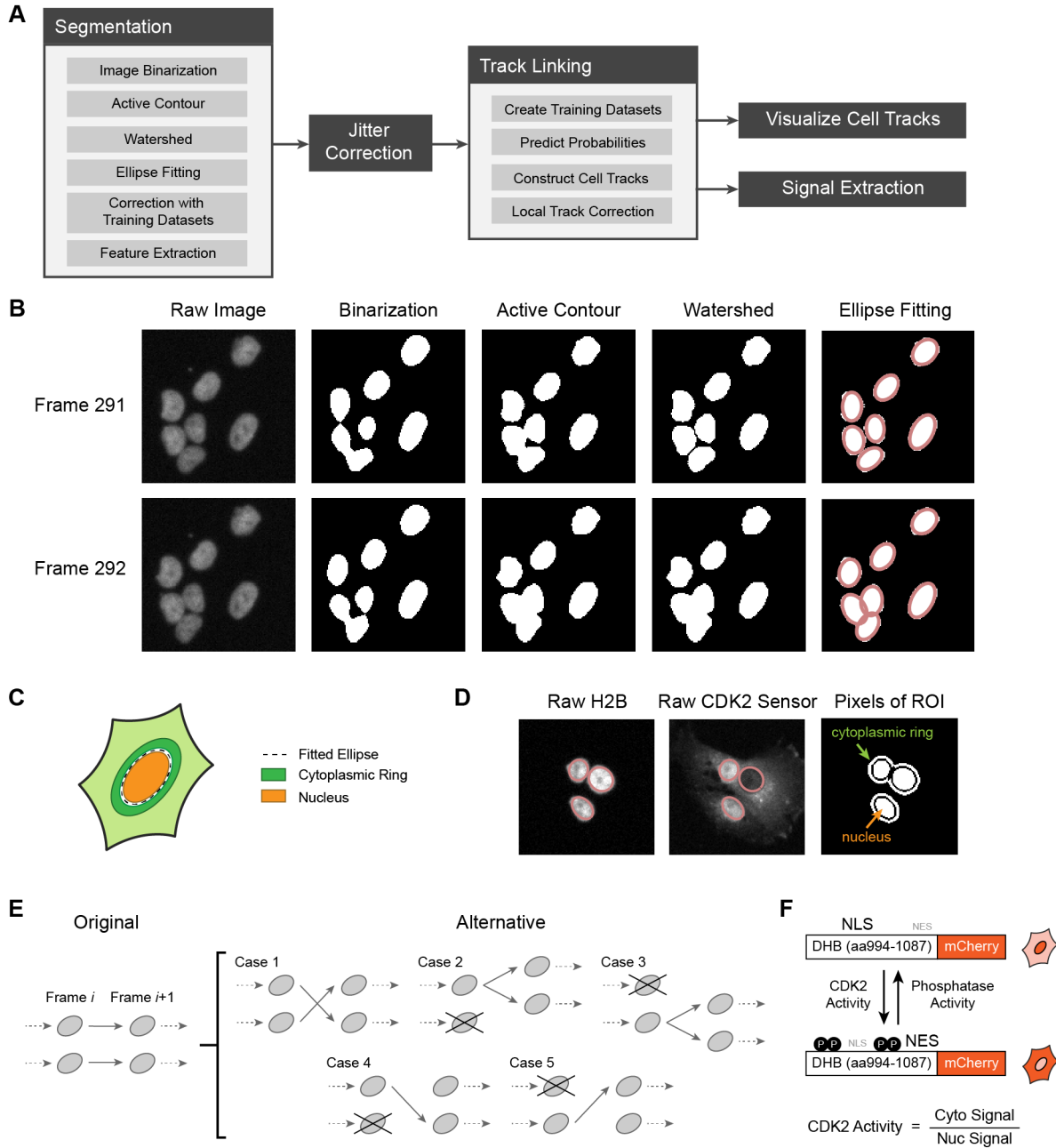


**Figure S1. Implementation of EllipTrack, related to Figure 1.**

(A) Schematic illustration of the EllipTrack workflow.

(B) Procedure of segmentation in EllipTrack. Raw images of the nuclear marker are first binarized. The binary images are then optimized with the Active Contour and Watershed algorithms. Finally, ellipses are fitted to the contours of the foreground pixels in the binary images. Dataset: A375-1.

(C) Schematic illustration of the nuclear and cytoplasmic ring.

(D) Visualization of the nucleus and cytoplasmic ring of overlapping nuclei. Left: Fitted ellipses plotted on top of the image of the nuclear marker (H2B). Middle: Fitted ellipses plotted on top of the CDK2 sensor image. Right:

Pixels used to define the nuclear and cytoplasmic rings (white). Pixels shared by multiple cells are removed from the calculation.

(E) Schematic illustration of the alternative track configurations for two cell tracks both mapping from one frame to the next. Case 1 will swap two cell tracks as done by the Magnusson swap operation. It aims to correct track swaps. Cases 2 and 3 will assign one cell track for mitosis and terminate the other one. They aim to detect missed mitosis events. Cases 4 and 5 will swap two cell tracks and then break one of them into pieces. They aim to remove unlikely migration events. These alternatives are chosen to correct the common tracking mistakes.

(F) Schematic illustration of the CDK2 sensor. DHB, DNA helicase B, a CDK2 substrate. NLS, Nuclear Localization Signal. NES, Nuclear Export Signal.

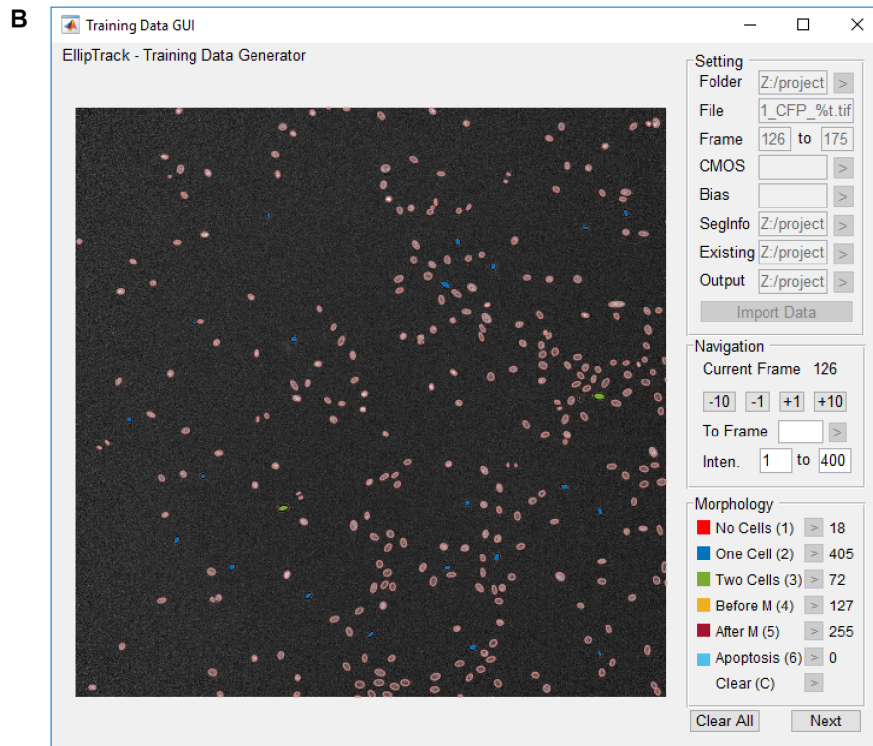
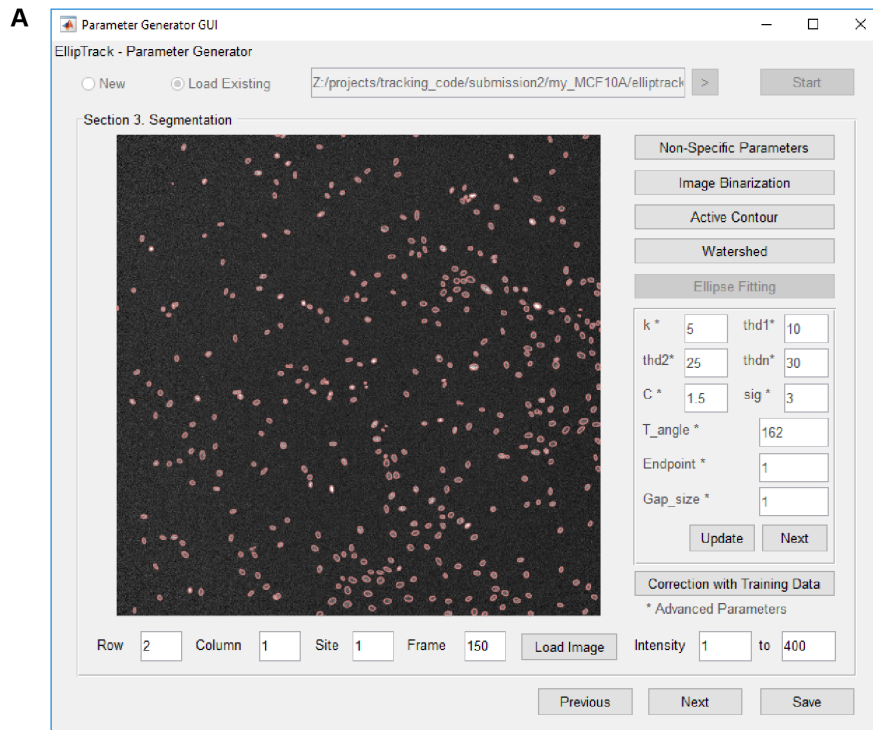


**Figure S2. Graphical User Interfaces, related to STAR Methods.**

(A) Parameter Generator GUI.

(B) Training Data GUI.

**SUPPLEMENTAL TABLES****Table S1. Comparison of cell trackers, related to Table 1.**

Cell Tracker	Segmentation	Track Linking	Post-Processing
EllipTrack	Thresholding/blob detection, active contour, watershed, ellipse fitting	Viterbi algorithm	Local track correction
Baxter Algorithm	Bandpass filter, watershed	Viterbi algorithm	Post-tracking segmentation
Cappell <i>et al.</i>	Thresholding/blob detection, watershed	Nearest neighbor. Terminate cell tracks when in doubt.	N/A
iLastik	Random forest classifiers	Flow-based algorithm	Post-tracking segmentation

**Table S2. Statistics of benchmarked movies, related to Table 1.**

A detection refers to one nucleus in one frame. “% Detections Annotated” indicates the percentage of detections that were manually annotated for constructing the ground truth cell lineages.

Movie	# Frames	# Cells in First Frame	# Cells in Last Frame	# Total Detections	Interval (min)	Duration (hr)	% Detections Annotated
HeLa-1	92	43	137	$8.6*10^3$	30	46	100
HeLa-2	92	125	363	$2.54*10^4$	30	46	100
BJ5TA	107	329	332	$3.54*10^4$	12	21.4	100
MCF10A-1	288	156	851	$1.17*10^5$	10	48	65
A375-1	482	50	318	$9.9*10^4$	15	120.5	100
RPE-hTERT	400	30	712	$1.05*10^5$	15	100	64

**Table S3. List of features, related to STAR Methods.**

Category	ID	Description	Remark
Ellipse Geometry	1	Area	$\pi ab$
	2	Major axis	Denote as $a$
	3	Minor axis	Denote as $b$
	4	Eccentricity	$\sqrt{a^2 - b^2}/a$
	5	Equivalent radius	Denote as $r = \sqrt{ab}$
	6	Approximate perimeter	$\pi\sqrt{2(a^2 + b^2)}$
	7	Adjusted radius	$ab/\sqrt{a^2 + b^2}$
Intensity of	8	Mean	Denote as $\mu_i$
Ellipse Interior	9	Standard deviation	Denote as $\sigma_i$
	10	Kurtosis	Denote as $\kappa_i$
	11	Median	Denote as $m_i$
	12	75% percentile	Denote as $q_i$
Intensity of	13	Mean	Denote as $\mu_b$
Ellipse Boundary	14	Standard deviation	
	15	Median	
	16	Ratio of internal to boundary intensity	$\mu_i/\mu_b$
	17	Approximate gradient	$(\mu_i - \mu_b)/r$
Intensity of	18	Intensity of ellipse centroid	Denote as $\mu_c$
Ellipse Centroid	19	Ratio of centroid to boundary intensity	$\mu_c/\mu_b$
	20	Approximate gradient	$(\mu_c - \mu_b)/r$
	21	Ratio of centroid to interior intensity	$\mu_c/\mu_i$
	22	Approximate gradient	$(\mu_c - \mu_i)/r$
Intensity Ratios of Ellipse Interior	23	Standard deviation / Mean	$\sigma_i/\mu_i$
	24	Kurtosis / Mean	$\kappa_i/\mu_i$
	25	Median / Mean	$m_i/\mu_i$
	26	75% percentile / Mean	$q_i/\mu_i$